Rotordynamics of a Vibroflot

Florian Tezenas Du Montcel, Sébastien Baguet, Marie-Ange Andrianoely, Régis Dufour, Stéphane Grange, Laurent Briançon, Piotr Kanty

Rotordynamics of a Vibroflot

Florian Tezenas du Montcel[1,3], Sébastien Baguet[1], Marie-Ange Andrianoely[1], Régis Dufour[1], Stéphane Grange[2], Laurent Briançon[2], Piotr Kanty[3]

[1] Univ Lyon, INSA Lyon, CNRS, LaMCoS, UMR5259, 69621 Villeurbanne, France
[2] Univ Lyon, INSA Lyon, GEOMAS, EA7495, 69621 Villeurbanne, France
[3] Menard, 22 rue Jean Rostand, 91400 Orsay, France
florian.tezenas-du-montcel@menard-mail.com

Abstract. This paper presents a modelling of a vibroflot dynamic behaviour. Vibroflots are used by ground improvement companies to perform vibro compaction. This technic consists in deeply densifying sandy soils by vibrations in order to make stable future infrastructures. A classical vibroflot is a slender structure composed of several rotors which are not rotating or driven by an asynchronous electrical motor that produces orbital vibration and therefore the soil compaction.
The final objective of the investigation is to establish a global multi-physics model coupling electromagnetic motor, rotordynamics and soil models in order, for example, to adjust the speed of rotation that generates the soil resonance, making the soil compaction easier.
The present paper presents only the electro-magnetic and mechanical models, in order to predict the vibroflot dynamic behaviour during the free hanging operation. Among the predicted results, the lateral displacement and motor amperage are of particular interest because they can be compared with the experimental measures collected on an in-situ full-scale instrumented vibroflot.

Keywords: Rotordynamics, Asynchronous electric motor, Multi-physics models, Vibroflot, Vibro compaction.

1. Introduction

Vibro compaction is a ground improvement technique which aims to deeply densify sandy soil in order to make stable future infrastructure [1]. It is used to control and reduce settlement, mitigate liquefaction [2], stabilize or treat hydraulic fill and limit lateral earth pressure behind quay walls. Loose soil can be compacted through insertion of vibrating probes, called vibroflots, together with a large volume of water. This enables the sand particles to rearrange themselves in a denser formation and thus increases the overall density of the soil. Vibro compaction is executed using a rig – excavator, drilling rig or crane –, a vibroflot, and auxiliary equipment such as generator, compressor, and water pumps. Under the effect of its own weight, the machine's pull-down force (if any), the effect of the jetted water and the sustained horizontal vibrations,

the vibrating probe rapidly reaches the desired depth. The probe is then gradually lifted in successive passes, producing in this way a cylinder of compacted ground (see Fig. 1).

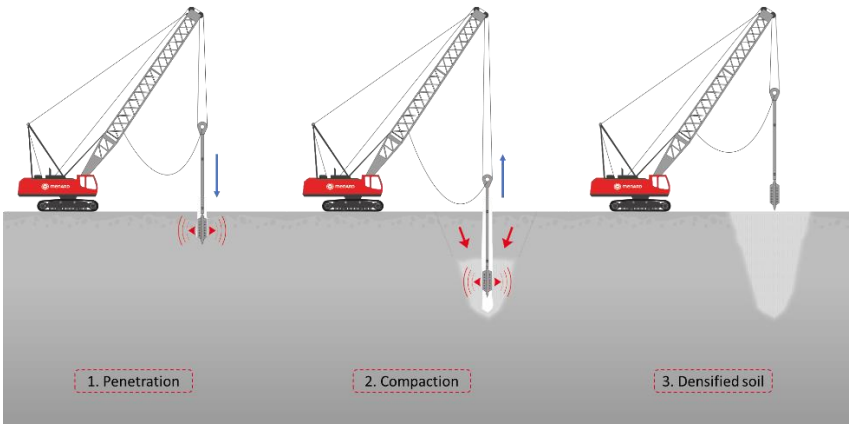

Fig. 1. Vibro compaction process.

Since the development of vibro compaction during the 1930s vibroflots were progressively improved following operational experiences. The current design can be described as a multirotor system coupled with a motor (see Fig. 2). A non-rotating tube casing, in contact with the soil, is supporting an eccentric rotor by means of rolling bearings. This internal rotor, driven in rotation by an electrical motor, produces orbital vibrations. This paper focuses on a vibroflot set in motion by an asynchronous electrical motor but vibroflots working with hydraulic motors also exist. To prevent the vibrations to be transmitted to the extension tubes and therefore to the rig, two rubber coupling parts are used to support the external tube and isolate the vibrations from the vibroflot.

It appears now necessary for soil improvement companies to accurately model this system to better know and improve their vibro compaction equipment and processes [3]. For instance, to be able to improve the lifetime of the equipment – bearings, rubber couplings, motor – and to improve vibro compaction process efficiency by working at resonance frequency [4]. This study was also motivated by the need to develop a new approach regarding vibro-compaction numerical models. Indeed, many studies, such as [5] or [6] are trying to simulate this particular soil improvement process but without any strong coupling between the soil and the vibroflot models – that is to say the amplitude and shape of vibrations are given to the soil model by the user. Others are seeing the importance to also model the vibroflot to better control vibro compaction process [7], but the model used is very simplified. The novelty presented here consists in model the vibroflot more accurately, including its electrical motor, which has not already been done.

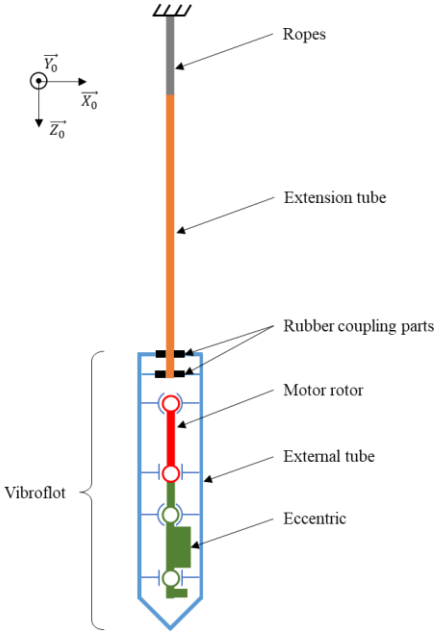

Fig. 2. Vibroflot kinematic scheme.

This paper presents only the vibroflot model in free hanging, which means without soil effects. At first the electrical model is described, then the multi-rotors model and the strong coupling made to solve both physics simultaneously are also presented. In a second part in-situ experimental investigations are described. Finally, numerical results are compared with in-situ measurements.

2. Numerical model

2.1. Electro-magnetic model

The asynchronous electrical motor modelled here is made of a three-phase wound stator with p pairs of poles, and a squirrel cage rotor. The magnetic circuit is supposed to be not saturated and has a constant permeability; ferromagnetic loss is negligible; and the influences of skin effect and heating are not taken into account on motor parameters.

Applying Lenz and Faraday electromagnetic laws to each stator and rotor phase the constitutive equations linking voltages and amperages are obtained. Then, after application of Park transformation [7], which consists in rewriting the tree-phase system into a two-phase model including only direct $\vec{d}$ and quadratic $\vec{q}$ axes, the set of four constitutive equation becomes:

$$
\begin{aligned}
v_{sd} &= R_s i_{sd} + \frac{d\emptyset_{sd}}{dt} - \frac{d\theta_s}{dt}\emptyset_{sq}\,, \\
v_{sq} &= R_s i_{sq} + \frac{d\emptyset_{sq}}{dt} + \frac{d\theta_s}{dt}\emptyset_{sd}\,, \\
v_{rd} &= R_r i_{rd} + \frac{d\emptyset_{rd}}{dt} - \frac{d\theta_r}{dt}\emptyset_{rq}\,, \\
v_{rq} &= R_r i_{rd} + \frac{d\emptyset_{rq}}{dt} + \frac{d\theta_r}{dt}\emptyset_{rd}\,,
\end{aligned}
\tag{1}
$$

with v, i, $\emptyset$, θ , R, stand respectively for the voltages, amperages, magnetic flux, angular positions, electrical resistance and with s, r, d, q subscripts refer respectively to the stator, rotor, direct axis, and quadratic axis. In this case, $(\vec{d},\vec{q})$ axes are oriented so that they are joined to the rotating field. Thus, the angular speed $\omega_s = \frac{d\theta_s}{dt}$ of $(\vec{d},\vec{q})$ axes in the stator coordinates, and the angular speed $\omega_r = \frac{d\theta_r}{dt}$, of $(\vec{d},\vec{q})$ axes in the rotor coordinates are defined. Furthermore, because of the squirrel cage, the voltage is applied only on the electrical stator and thus $v_{rd} = v_{rq} = 0$.

In these conditions the electromagnetic parameters are reduced to five: L_s the stator inductance, L_r the rotor inductance, M the mutual inductance between the stator and the rotor, $T_r = \frac{L_r}{R_r}$ the rotor time constant, and $\sigma = 1 - \frac{M^2}{L_r L_s}$ the total leakage factor. Finally, introducing the magnetic flux expression, Eq. (1) is rewritten in a matrix form, such as:

$$
\{v\} = [B]\frac{d}{dt}\{i\} + [A]\{i\}\,, \tag{2}
$$

with $[A]$ and $[B]$ matrices depending on stator and rotor parameters, as well as $(\vec{d},\vec{q})$ axes angular speeds. To simplify equations, the following changes of variables are stated: $i'_{rd} = \frac{L_r}{M} i_{rd}$ and $i'_{rq} = \frac{L_r}{M} i_{rq}$. Solving Eq. (2) provides the four electrical intensities and therefore the electrical torque:

$$
C_m = p(1-\sigma)L_s\left(i_{sq} i'_{rd} - i_{sd} i'_{rq}\right), \tag{3}
$$

that permits a strong coupling between electromagnetic and mechanical models.

In order to access motor parameters easily, on a first estimation, nameplate information is used [8]. Indeed, these properties are not directly available for this kind of motor. It should be noted that the parameters are supposed constant, at least close to the nominal working state. More precise techniques could have been used but would have required electro-mechanical measurements or more complex identification methods.

Only the stator resistance R_s is measured. Then, the other parameters are estimated as follows:

$$\sigma = \frac{1 - \cos(\varphi_n)}{1 + \cos(\varphi_n)}, \tag{4}$$

$$\omega_{sln} = 2\pi f_{sn} - N_{rn} p \frac{2\pi}{60}, \tag{5}$$

$$T_r = \frac{1}{\sqrt{\sigma}\omega_{sln}}, \tag{6}$$

$$L_s = \frac{\sqrt{\sigma} V_{sn}}{I_{sn} 2\pi f_{sn}} \left(1 + \frac{1 - \sigma}{\sigma}\right), \tag{7}$$

with φ_n the nominal power factor, f_{sn} the nominal stator electric frequency, N_{rn} the nominal rotor speed, V_{sn} the nominal voltage, and I_{sn} the nominal amperage.

2.2. Multi-rotor model

Multi-rotor model permits simulating the transient dynamic behaviour of the three rotors composing the vibroflot. The rotordynamics theory is inspired from [9], [10] and [11]. Each rotor shaft is modelled by 1D Timoshenko finite elements taking into account, on each node, the six degrees of freedom devoted to bending, axial and torsion motions. Two-node bearing, and two-node nonlinear rubber coupling FE are also available. Furthermore, in this case-study, mass unbalance and gravity are considered. Finally, after the assembly, the application of the Lagrange equations yields the multi-rotor equation of motion:

$$\begin{aligned} [M_S]\{\ddot{q}\} + (\dot{\varphi}[G_S] + [C_b])\{\dot{q}\} + \left(\ddot{\varphi}[D_S] + [K_S] + \left[K_{gS}\right] + [K_b]\right)\{q\} \\ = \ddot{\varphi}\{F_{kS}\} + \{F_u\} + \left\{F_{gS,t}\right\} + \{F_{kb}\} + \{F_{km}\}, \end{aligned} \tag{8}$$

with $[M_S]$ the shafts mass matrix, $[G_S]$ the shaft gyroscopic matrix, $[C_b]$ the rolling bearings damping matrix, $[D_S]$ the shafts kinetic stiffness matrix, $[K_S]$ the shafts stiffness matrix, $\left[K_{gS}\right]$ the shafts gravity matrix, $[K_b]$ the rolling bearings damping matrix, $\{F_{kS}\}$ the shaft torsion kinetic force vector, $\{F_u\}$ the unbalance force vector, $\left\{F_{gS,t}\right\}$ the shafts gravity traction force vector, $\{F_{kb}\}$ the bearings resistive torque vector, $\{F_{km}\}$ the motor torque vector, $\dot{\varphi}$ the speed of rotation of the internal rotor, and $\{q\}$ the vector containing all rotors degrees of freedom.

2.3. Global model assembly

The global system consists of the electro-magnetic first order differential equations and of the mechanical second order differential equations. Coupling strongly the models requires to rewrite the system of equation as a Cauchy problem: $\dot{y}(t) = f\big(t, y(t)\big)$ and to solve all equations together at each time step. With the following change of variables:

$$Y^T = \langle \{q\} \quad \{\dot{q}\} \quad \{i\} \quad \varphi \quad \dot{\varphi} \rangle \tag{9}$$

the global system related to Eqs. (2), (3) and (8) becomes:

$$\dot{Y} = \begin{bmatrix} \{Y(2)\} \\ [M]^{-1}(-[C]\{Y(2)\} - [K]\{Y(1)\} + \{F\}) \\ [B]^{-1}(\{v\} - [A]\{Y(3)\}) \\ \{Y(4)\} \\ \big(C_m(\{Y(3)\}) - C_r(\{Y(4)\})\big)/I_P \end{bmatrix} \tag{10}$$

Then the time integration of the coupled models is carried out using Matlab ODE15s solver [12], which is a variable-step, variable-order (VSVO) solver based on the numerical differentiation formulas (NDFs) of orders 1 to 5. After defining all rotors and motor parameters the only input variable is the voltage applied between the motor phases.

The predicted results presented in section 4 are obtained with 6 degrees of freedom for the electro-magnetic model and with 345 degrees of freedom for the finite element model. Thus, the length of vector Y defined in Eq. (10) is 696.

3. In-situ experimental investigation

To validate the numerical model, an in-situ measurement campaign was conducted on a full-scale experiment V23 vibroflot. The whole process was instrumented but only the measurements related to the models discussed previously are presented in what follows. Sensors were fixed on the vibroflot, and on the electrical cabinet to monitor the dynamic behaviour of the vibroflot hung above the ground. Five triaxial accelerometers were used with a 2 kHz sampling frequency: three fixed on the external tube of the vibroflot and two fixed at the bottom of the extension tube (see Fig. 3). To access vibroflot's displacements in 3D the accelerations recorded are integrated using a Newmark scheme with high-pass filters.

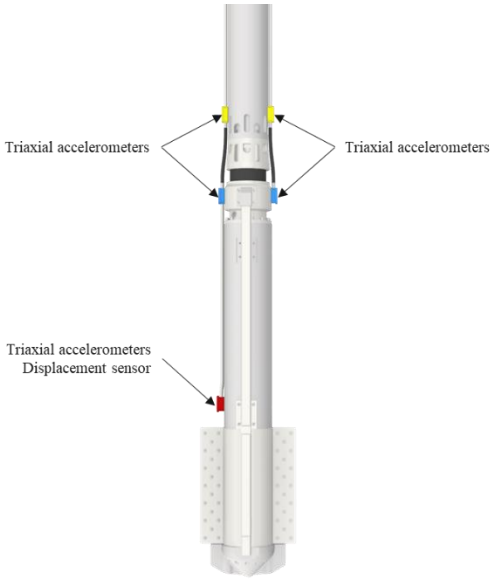

Fig. 3. Position of sensors fixed on the instrumented vibroflot.

To measure the rotation speed of the internal rotor an eddy current displacement sensor was fixed in front of a ten teeth wheel. Then the speed is calculated by detecting rising edges. In order to have accurate data of changing speeds the sampling frequency was 20 kHz.

Motor amperage – effective value – and frequency were directly measured by the frequency inverter used to control the vibroflot and recorded by the same data acquisition system as the other sensors respectively at 200 Hz and 100 Hz.

4. Results and comparison with in-situ measurements

The predicted results are compared with the measurements carried out on site. Motor output state after start-up is summarized in Table 1. Simulated rotational speed and amperage values in steady state are satisfactory, especially since the motor parameters are roughly estimated.

Table 1. Comparison of motor parameters at 60 Hz in steady state.

Parameter	Measured value	Simulated value	Relative gap
Rotational speed	1795 rpm	1789 rpm	-0,3 %
Amperage	76 A	75 A	-1,3 %

Regarding the multi-rotors model, results are also close to the real vibroflot's behaviour. Fig. 4 clearly shows the double cone shape of vibration, with the highest amplitude at the tip of the vibroflot. Tip and top amplitudes are of the same order as the measured ones.

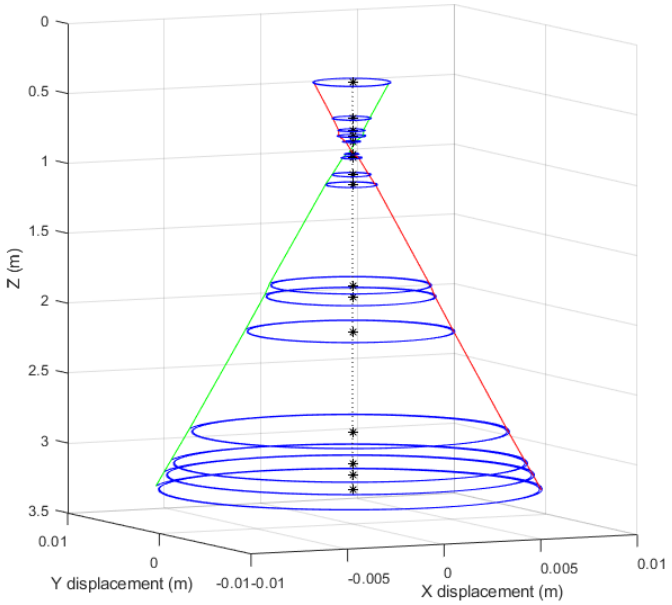

Fig. 4. Orbits and vibration envelope of the external tube of the vibroflot set in motion by its electrical motor operating at 60 Hz – numerical results.

5. Conclusion and perspectives

The prediction of the transient dynamic behaviour of a vibroflot hung above the ground has been numerically simulated using a model coupling strongly the electro-magnetic model based on the Park transformation and the mechanical model based on 1D-elements. These models take the gravity force into account and are able to reproduce the global shape of vibration of the vibroflot by applying only a voltage between the electrical stator model phases.

This model can still be improved by implementing a more complex model for predicting bearing moment loss. Moreover, motor parameters were only estimated, on a first approach, by simplified formulations. To increase the global model accuracy at different frequencies motor parameters must be better defined.

The next step is devoted to the prediction of the vibroflot behaviour during vibro compaction in a sandy soil, using the developed electro-mechanical finite element model.

Acknowledgements

The authors would like to thank Menard company for its financial and technical support, Pr. Xuefang Lin-Shi for her advice.

References

1. Kirsch, K., Kirsch, F.: Ground Improvement by Deep Vibratory Methods. 2nd edn. CRC Press, U.S (2017).
2. Debats, J.M., Mollereau, C.: Ground improvement and reinforcement in seismic zones by vibrocompaction and stone columns. Géo Montréal (2013).
3. Nagy P.: Deep Vibro Compaction - Dynamic Compaction Control Based on the Vibrator Movement. PhD thesis, Vienna University of Technology (2018).
4. Massarch, K.R, Zackrisson, P., Fellenius, B.H: Underwater resonance compaction of sand fill. In: 19th International Conference on Soil Mechanics and Geotechnical Engineering Proceedings. Seoul (2017).
5. Nagula, S.S., Grabe, J.: Coupled Eulerian Lagrangian based numerical modelling of vibrocompaction with model vibrator. Computers and Geotechnics (2020).
6. Triantafyllidis, Th., Kimmig, I.: A simplified model for vibro compaction of granular soils. Soil Dynamics and Earthquake Engineering (122), 261–276 (2019).
7. Nagy, P., Adam, D.: Quality control of deep vibro compaction based on the vibrator movement. In: XVII ECSMGE-1019 Proceedings. Geotechnical Engineering foundation of the future (2019).
8. Kostenko, M., Piotrovski, L.: Machines électriques : Tome 2 : Machines à courant alternatif. Edition Mir, Moscow (1969).

9. Boglietti, A., Ferraris, P., Pastorelli, M., Profumo, F., Zimagliac, C.: Induction Motors Field Oriented Controllers using data sheets motor parameters. International Conference on Electrical Machine (ICEM), vol. 2, pp. 656-660. Paris (1994).
10. Nelson, H.D.: A Finite Rotating Shaft Element Using Timoshenko Beam Theory. ASME Journal of Mechanical Design (102), pp. 793-803 (1980).
11. Lalanne, M., Ferraris, G.: Rotordynamics Prediction in Engineering. 2nd edn. Wiley, England (2011).
12. Nguyen K. L., Tran Q. T., Andrianoely M-A., Manin L., Dufour R., Baguet S., Mahjoub M., Menand S.: Nonlinear rotordynamics of a drillstring in curved wells: models and numerical techniques. International Journal of Mechanical Sciences, 166-105225 (2020).
13. Shampine, L. F, Reichelt, M. W.: The MATLAB ODE Suite. SIAM Journal on Scientific Computing (18), 1–22 (1997).